Nanoscale

PAPER

View Article Online
View Journal | View Issue

Cite this: *Nanoscale*, 2022, **14**, 7242

Nature of the 1/*f* noise in graphene—direct evidence for the mobility fluctuation mechanism†

Adil Rehman, *[a] Juan Antonio Delgado Notario, [a] Juan Salvador Sanchez, [b] Yahya Moubarak Meziani, [b] Grzegorz Cywiński, [a] Wojciech Knap,[a] Alexander A. Balandin, *[c] Michael Levinshtein [d] and Sergey Rumyantsev *[a]

Received 12th January 2022,
Accepted 11th April 2022

DOI: 10.1039/d2nr00207h

rsc.li/nanoscale

The nature of the low-frequency 1/*f* noise in electronic materials and devices is one of the oldest unsolved physical problems (*f* is the frequency). The fundamental question of the noise source—fluctuations in the mobility *vs*. number of charge carriers—is still debated. While there are several pieces of evidence to prove that the 1/*f* noise in semiconductors is due to the fluctuations in the number of the charge carriers, there is no direct evidence of the mobility fluctuations as the source of 1/*f* noise in any material. Herein, we measured noise in an *h*-BN encapsulated graphene transistor under the conditions of geometrical magnetoresistance to directly assess the mechanism of low-frequency electronic current fluctuations. It was found that the relative noise spectral density of the graphene resistance fluctuations depends non-monotonically on the magnetic field (*B*) with a minimum at approximately $\mu_0 B \cong 1$ (μ_0 is the electron mobility). This observation proves unambiguously that mobility fluctuations are the dominant mechanism of electronic noise in high-quality graphene. Our results are important for all proposed applications of graphene in electronics and add to the fundamental understanding of the 1/*f* noise origin in any electronic device.

Introduction and problem statement

The history of 1/*f* noise investigation started in 1925, almost a hundred years ago, when Johnson discovered that fluctuations of the thermionic current in a vacuum tube increase with frequency decrease.[1] Since that time, 1/*f* noise has been discovered in an enormous number of electronic and non-electronic systems. It is conventionally accepted that the term "1/*f* noise" is applied to fluctuations with the smooth $1/f^{\gamma}$ spectrum with the slope parameter $\gamma \cong 0.8$–1.2. It was soon established that the noise spectral density of the current fluctuations in semiconductor and metal resistors in the linear regime is proportional to the voltage squared (see reviews,[2–5] and references therein). This fact suggests that the 1/*f* noise is due to the resistance fluctuations, and the electrical current only reveals these fluctuations. In 1976, more than fifty years since the discovery of the 1/*f* noise, the direct proof of resistance fluctuations as an origin of the 1/*f* noise was provided by Voss and Clark.[6] They demonstrated that the slow fluctuations of the thermal noise amplitude and the fluctuations of the current are caused by the same equilibrium fluctuations of the resistance. Moreover, the amplitude and spectrum of the resistance fluctuations were the same in both experiments.

The next important fundamental question to be answered is: what causes these resistance fluctuations? It can be either the fluctuations in the mobility of the charge carriers or their number. This is not an easy question because the mobility and concentration of the charge carriers contribute symmetrically to resistance $R \sim 1/N\mu$ (N is the number of charge carriers and μ is the mobility). The contribution of mobility and the fluctuations in the number of carriers can be different depending on the devices and materials. For example, the McWhorter model describes accurately the 1/*f* noise in many semiconductor devices by attributing it to the fluctuations in the number of charge carriers.[7] While many studies attribute noise in metals or certain electronic devices to mobility fluctuations, the evidence for such fluctuations as the true source of the 1/*f* noise is more controversial. One should emphasize that the question of 1/*f* noise origin is important not only for fundamental

[a]*CENTERA Laboratories, Institute of High Pressure Physics, Polish Academy of Sciences, Warsaw 01-142, Poland. E-mail: adilrehman@gmail.com, roumis4@gmail.com*
[b]*Nanotechnology Group, USAL-Nanolab, Universidad de Salamanca, Salamanca 37008, Spain*
[c]*Nano-Device Laboratory, Department of Electrical and Computer Engineering, University of California, Riverside, California 92521, USA. E-mail: balandin@ece.ucr.edu*
[d]*Ioffe Physical-Technical Institute, St. Petersburg 194021, Russia*
† Electronic supplementary information (ESI) available. See DOI: https://doi.org/10.1039/d2nr00207h

science but also for practical electronic applications that require low noise levels or use noise measurements for assessing materials' quality or device reliability.[8–12]

Fluctuations in the number of charge carriers as the source of 1/*f* noise in semiconductors

The theory of electron transport in a magnetic field provides an elegant way for testing the nature of 1/*f* noise. In 1983, some of us used noise measurements in a magnetic field in order to distinguish between the mobility ($\delta\mu$) and the fluctuations in the number of carriers (δN).[13] In the sample geometry with the length (L) much smaller than its width (W), *i.e.*, $L \ll W$, or in the Corbino disc geometry, the magnetic field (B) perpendicular to the electrical field causes the well-known effect of geometrical magnetoresistance[14–16]

$$\rho_{xx} = \rho_0[(1 + (\xi\mu_0 B)^2]. \quad (1)$$

Here ρ_{xx} is the longitudinal resistivity, ρ_0 and μ_0 are the resistivity and mobility at B = 0 T, and ξ is the scattering factor, which depends on the details of the scattering mechanisms, *e.g.*, in semiconductors, $\xi \geq 1$. Differentiating eqn (1), one can show that the mobility fluctuations do not contribute to the resistance fluctuations when the condition $\xi\,\mu_0 B = 1$ is satisfied:

$$\frac{\delta\rho_{xx}}{\rho_{xx}} = \frac{\delta\mu_0}{\mu_0}\frac{(\xi\mu_0 B)^2 - 1}{(\xi\mu_0 B)^2 + 1}. \quad (2)$$

Therefore, if the 1/*f* noise is caused by mobility fluctuations, then one can expect a strong decrease in noise at $\mu_0 B \cong 1$. On the other hand, the concentration and the total number of carriers do not depend on the magnetic field, and the noise, in the case of the dominance of the fluctuations in the number of carriers, should not depend on the magnetic field.

The measurement of 1/*f* noise in a semiconductor, such as GaAs, under the condition of strong geometrical magnetoresistance, showed that the noise does not depend on the magnetic field.[13] The latter led to the conclusion that the fluctuations in the number of charge carriers were the source of the 1/*f* noise. It was also shown that the noise was not originating on the surface of the semiconductor but rather in its volume. Similar experiments with the same conclusions have been repeated by other groups for GaAs and by some of us for GaN.[17–21] Other investigations on the nature of noise in semiconductors also complied with the fluctuations in the number of carriers as the source of the 1/*f* noise. Among the alternative experimental evidence, one can indicate the gate voltage dependence of noise in the field-effect transistors (FETs), especially in n-channel Si metal–oxide–semiconductor field-effect transistors (MOSFETs). It is conventionally accepted that, with rare exceptions, the 1/*f* noise in MOSFETs complies with the McWhorter model, which assumes the fluctuations in the number of carriers. This model predicts, and the experiments confirm, in the majority of cases, that when the concentration (n_s) in the channel is tuned by the gate voltage, the noise depends on concentration as $1/{n_s}^2$. Another notable proof of the carrier–number fluctuations demonstrated that individual defects in microstructures cause random telegraph signal (RTS) noise due to charge carrier trapping and de-trapping.[22] The level of this type of noise differed from device to device due to the statistical variance in the number and properties of the defects. Averaging the noise spectra from several dozen devices yielded the same 1/*f* noise spectrum as the one measured in larger devices obtained *via* the same fabrication process. These results allowed the authors to conclude that "There can now be no doubt that measurements of noise and RTSs in microstructures have shown definitively that l/*f* noise in MOSFETs and MIM tunnel diodes is generated through carrier trapping".[22]

Fluctuations in the mobility of charge carriers as a possible source of 1/*f* noise

While numerous trusted experiments demonstrate that the 1/*f* noise in semiconductors relates to the fluctuations in the number of charge carriers, there is no direct and conclusive evidence for the mobility fluctuations as a source of 1/*f* noise in any material system. On the other side, it is generally accepted now that the physical origin of the 1/*f* noise is not universal and may differ from one material system to another (see for example ref. 4). Therefore, it is possible that noise in some materials and devices can be of mobility fluctuation origin. There have been attempts by some of us for reproducing the experiments of noise measurement under the conditions of strong geometrical magnetoresistance for the materials in which mobility fluctuations may dominate the 1/*f* noise. For a long time, the best candidates for such materials were considered to be metals.[4] However, it is difficult to satisfy the condition $\mu B = 1$ in metals for a reasonable magnetic field owing to the low electron mobility in metals at room temperature (RT). Cooling down the metals increases the electron mobility but also decreases the resistivity, making the noise measurements extremely challenging, especially for the samples with the $W \gg L$ geometry. Some of us have made several attempts to measure noise in metals at low temperatures in a strong magnetic field but failed to obtain conclusive results.

In 2004, a new opportunity emerged for proving directly a possibility of the mobility-fluctuation nature of the 1/*f* noise. The latter came with the exfoliation of graphene, characterized by many unique properties.[23–25] Among them are the high charge carrier mobility at RT and unusual 1/*f* noise behaviour. A large number of reports devoted to the low-frequency noise in graphene have been published (see ref. 26 and references therein). The electronic noise was typically studied in back-gated or top-gated graphene FETs. It was found that the gate-voltage dependence of the noise can be different in different graphene devices, especially close to the charge neutrality point, described by the "V", "M" and "Λ" shapes of the noise spectral density dependence on the gate-voltage. The important conclusion from all the studies was that the overall gate-voltage dependence of noise in graphene FETs is weak, and it does not comply with the McWhorter model. This observation led to the suggestion that mobility fluctuations can possibly constitute the physical mechanism of the 1/*f* noise in graphene.[27]

A scenario when the mobility fluctuations are responsible for the 1/*f* noise can be envisioned theoretically. The latter can be a result of the scattering cross-section fluctuations. In the case of only one type of fluctuating scattering center, the noise spectral density of the resistance fluctuations is given as[28,29]

$$\frac{S_R}{R^2} = \frac{4N_{t\mu}}{V}\frac{\tau P(1-P)}{1+(\omega\tau)^2} l_0{}^2(\sigma_2-\sigma_1)^2 \quad (3)$$

where $N_{t\mu}$ is the concentration of the scattering centers of a given type, V is the volume, l_0 is the mean free path of the carriers, P is the probability for a scattering center to be in the state with the cross-section σ_1, and τ is the characteristic time constant. There can be different reasons for fluctuations in the scattering cross-section, *e.g.*, change of the traps' charge state, the motion of the dislocations and individual atoms, or the diffusion of defects. Since these processes can have different values of τ, σ, and P, the integration over these parameters leads to the 1/*f* or 1/*f*-like noise spectrum. One should note that the relative noise spectral density in eqn (3) does not depend on either the free carrier concentration or the total number of carriers in the sample. This complies with the weak gate-voltage dependence observed for the low-frequency noise in graphene FETs.[30] Another indirect indication that the 1/*f* noise in graphene can be of the mobility fluctuation origin was obtained in the experiments with graphene FETs irradiated with the electron beam.[31] As expected, the irradiation resulted in the introduction of additional defects and the reduction of electron mobility, as was observed by other groups as well (see, for example ref. 32). Surprisingly, irradiation led also to a decrease in the 1/*f* noise level. This unusual behavior of the 1/*f* noise in graphene can be explained if one assumes the mobility fluctuation mechanism and adopts eqn (3). Indeed, the radiation-induced introduction of defects leads to a decrease in the mobility and mean free path, with a corresponding decrease in noise. One should note here that the defects, which mostly limit the electron mobility and the scattering centers predominantly responsible for the 1/*f* noise are not necessarily the same. Similar results were obtained by other independent research groups using different types of irradiation.[33,34]

The prior studies on noise in graphene suggested that this material is an excellent candidate for demonstrating directly that the mobility fluctuations can be the mechanism of the 1/*f* noise *via* experiments with a magnetic field. In 2013, some of us made the first attempt at such a study.[35] The reduction of the 1/*f* noise in graphene FETs subjected to a magnetic field was observed at cryogenic and near RT temperatures. However, the noise dependence on the magnetic field strength was different from that predicted by eqn (1). The studied graphene samples were also characterized by strong physical rather than geometrical magnetoresistance. The possible reason for that could be the high concentration of the defects in the studied samples and a rather low charge carrier mobility. Therefore, the conclusion of the nature of the 1/*f* noise could not have been made at that time.

To sum up, the multiple prior efforts at demonstrating that the mobility fluctuations can be the dominant source of the 1/*f* noise in any electronic material system have failed. One can only state that there have been experiments suggesting indirectly that the 1/*f* noise can be of the mobility fluctuation type in graphene. These are the experiments with the gate-bias dependence and irradiation effects on noise mentioned above. In this work, we studied the 1/*f* noise in graphene in a magnetic field and proved that it is indeed caused by mobility fluctuations. This is the first proof that mobility fluctuations can be a source of the 1/*f* noise in electronic systems.

Results and discussion

Device structure and current–voltage characteristics

For this study, we used high-quality single layer graphene encapsulated in *h*-BN to fabricate back-gated FETs. The device design and high-quality graphene allowed us to achieve an electron mobility of ~3 $m^2 V^{-1} s^{-1}$ at room temperature. It is important that such a high mobility value was achieved in graphene FETs on substrates, rather than suspended graphene, to ensure proper gating and Fermi level tuning. The measurements were intentionally performed at relatively high temperatures of 200 K–300 K in order to avoid complications in data interpretation due to the quantum confinement effects possible at low temperatures. The aspect ratio of the FET rectangular channel was chosen to be relatively small ($W/L = 4$). In comparison with a higher W/L ratio, these specific dimensions allowed us to minimize the contribution of the contact resistance. Fig. 1a and b show the schematic of the *h*-BN encapsulated transistor and the optical microscope image of the two representative devices, respectively. The current–voltage (*I*–*V*) characteristics and the low-frequency noise were measured inside the closed cycle cryogenic probe station using conventional instrumentation (Lake Shore). Fig. 1c presents the transfer *I*–*V* characteristics of the graphene FET measured at two temperatures. It is seen that the Dirac charge neutrality voltage (V_D), does not depend on temperature. Away from the Dirac point, there is a region of bias voltage where the *I*–*V* characteristics are linear. The *I*–V_s start to saturate at higher voltages. There are several possible reasons for this saturation.[36,37] One of them, most relevant in the context of the present study, is the contact resistance (R_c), which may become comparable with the channel resistance at high carrier concentration.

The upper bound of the contact resistance can be estimated by assuming a concentration independent mobility. In this case, the extrapolation of the resistance *versus* $(V_D - V_G)^{-1}$ dependence to $(V_D - V_G)^{-1} = 0$ yields a rough estimate of the total contact resistance. Using this procedure, we obtained $R_c = 100\ \Omega$ and 140 Ω at temperatures 300 K and 200 K, respectively (at $B = 0$ T). These values correspond to the contact resistivity of 2000 Ω μm and 2800 Ω μm, which are within the range reported for the graphene metal contacts.[38] Analysis of the current–voltage characteristics in the magnetic field showed that the contact resistance does not increase in the magnetic field (Fig. S1†). The

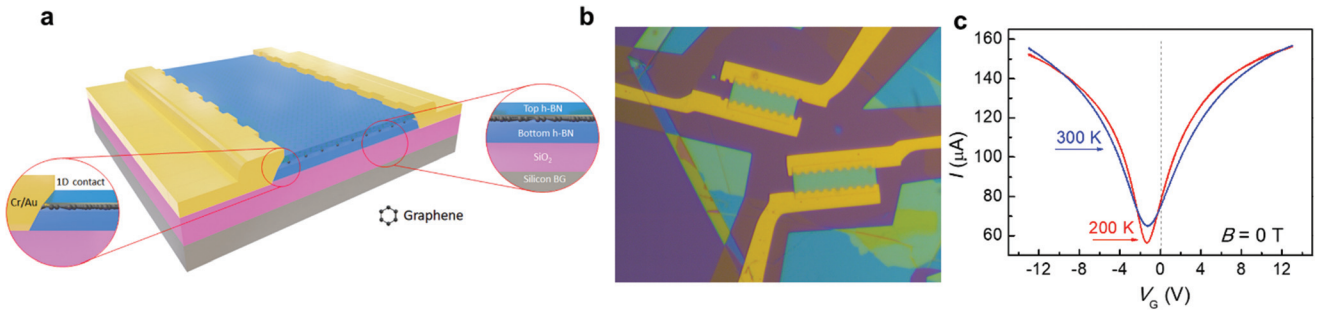

Fig. 1 Graphene device design and current–voltage characteristics. (a) Schematic and (b) optical microscopy image of *h*-BN encapsulated graphene FETs used in the study. (c) Transfer current–voltage characteristic of the representative graphene FET. The transfer I–V_G plots are shown for 300 K and 200 K. The vertical dashed line indicates the bias voltage used for the noise measurements.

noise was measured at $V_G = 0$. This bias point corresponds to the linear part of the I–V characteristic that ensures the small effect of the contact resistance. Based on the location of this bias voltage with respect to the Dirac point, the electrons dominated the electrical conductivity and noise properties.

Magnetoresistance and noise spectra

It is known that in graphene the magnetoresistance can show a complicated behavior with the magnetic field (B) with the dependencies ranging from $\sqrt{B}$ to B^2. The type of dependence is defined by the specific scattering mechanisms, which limit electron transport.[39,40] Recent detailed measurements of magnetoresistance in Corbino disks fabricated from high quality suspended graphene demonstrated the quadratic dependence of the magnetoresistance.[40] These results confirm the validity of eqn (1), at least for the specific scattering mechanisms. The results of our magnetoresistance measurements are presented in Fig. 2a and b. To analyze the results, we take into account the contact resistance and a finite W/L ratio:

$$R(B) = R_{Ch}[1 + (\eta\xi\mu_0 B)^2] + R_c. \quad (4)$$

Here R_{Ch} is the resistance of the channel without a magnetic field ($B = 0$ T), R_c is the total contact resistance, and η is the geometrical factor. In small magnetic fields $\mu_0 B < 1$, the geometrical factor can be approximated as $\eta^2 = (1 - 0.54L/W)$.[15] One can see in Fig. 2a, that in a weak magnetic field, the relative magnetoresistance, indeed, depends quadratically on the magnetic field, *i.e.* $[R(B) - R(0)]/R(0) \sim B^2$. In high magnetic fields, this dependence becomes weaker (see Fig. 2b) so that it can be approximated as $[R(B) - R(0)]/R(0) \sim B$. There are several reasons for the deviation from the quadratic magnetoresistance, which include the dependences of the momentum relaxation time and the cyclotron frequency on the magnetic field, as well as the influence of the sample borders. The analysis of the magnetoresistance in a high magnetic field in graphene is beyond the scope of the present work.

Eqn (4) can be used to estimate the mobility. Since the values of the parameters η, ξ and R_c are unknown, only the apparent mobility can be estimated:

$$\eta\xi\mu_{app} = \left(\frac{R(B) - R_{Ch} + R_c}{R_{Ch} + R_c}\frac{1}{B^2}\right)^{0.5}. \quad (5)$$

The actual mobility μ_0 can be either smaller or higher than the $\eta\xi\mu_{app}$ value depending on the η, ξ and R_c parameters. As will be shown later, the actual value of the mobility is not required for noise analysis.

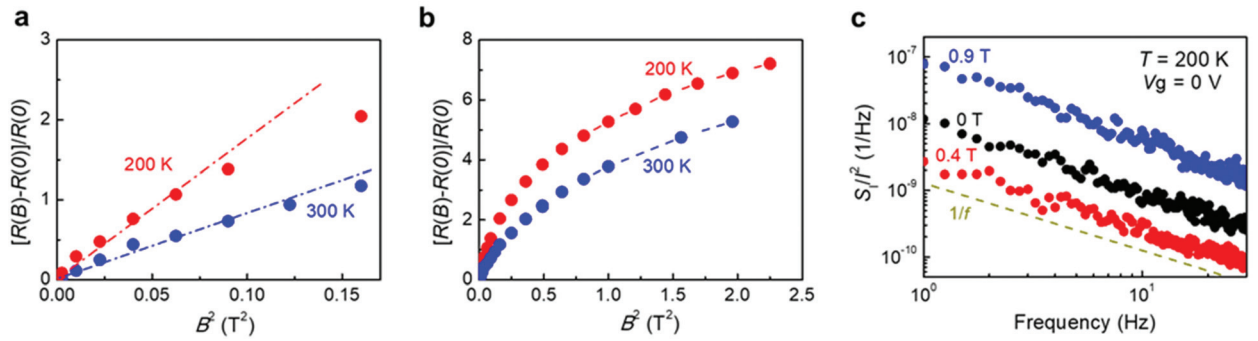

Fig. 2 Relative magnetoresistance as a function of the magnetic field and examples of the noise spectra. The $[R(B) - R(0)]/R(0)$ dependence is shown in the (a) low and (b) high magnetic fields at temperatures of 300 K and 200 K. (c) Noise spectra are shown at 200 K at different magnetic fields.

From the measured data, we obtained $\eta\xi\mu_{app} \cong 3\ m^2\ V^{-1}\ s^{-1}$ at 300 K and $\eta\xi\mu_{app} \cong 3.8\ m^2\ V^{-1}\ s^{-1}$ at 200 K. The actual electron mobility relates to the apparent mobility as

$$\mu_0{}^2 = \mu_{app}{}^2 \frac{R_{Ch} + R_c}{R_{Ch}}. \quad (6)$$

The resistance fluctuations owing to the mobility fluctuations can be obtained by differentiating eqn (4), resulting in the expression:

$$\frac{\delta R(B)}{R(B)} = \frac{\delta\mu_0}{\mu_0}\left[\frac{(\eta\xi\mu_0 B)^2 - 1}{(\eta\xi\mu_0 B)^2 + 1 + R_c/R_{Ch}}\right]. \quad (7)$$

The noise spectral density, corresponding to these resistance fluctuations, can be obtained by taking a square of eqn (7) and replacing actual mobility with the apparent one, in accordance with eqn (6). We also assume that the squares of the fluctuations $\delta\mu_0$ and $\delta R(B)$ represent their spectral noise densities:

$$\frac{S_R(B)}{R(B)^2} = \left[\left(\frac{R_{Ch}}{R_{Ch} + R_c}\right)^2 \frac{S_{\mu_0}}{\mu_0{}^2}\right] \left[\frac{\left(\eta\xi\mu_{app}B\right)^2 \frac{R_{Ch} + R_c}{R_{Ch}} - 1}{\left(\eta\xi\mu_{app}B\right)^2 + 1}\right]^2 + C. \quad (8)$$

Here, we added a constant (C) that represents the residual noise remaining when the noise due to the mobility fluctuations is suppressed. The first factor in eqn (8) is the noise at a zero magnetic field. The parameter $\eta\xi\mu_{app}$ is known from the magnetoresistance measurements. Therefore, the fitting parameters in eqn (8) are the contact resistance (R_c) and the residual noise level (C). The upper bound of the contact resistance is known from the I–V characteristics.

The low-frequency noise spectra measured at 300 K and 200 K were always of the $1/f^{\gamma}$ type with $\gamma \sim 1$. Fig. 2c shows a few examples of the noise spectra measured at 200 K and in different magnetic fields. The noise spectral density of the resistance fluctuations only weakly depended on the gate voltage and was independent of the drain voltage.

Noise in the magnetic field

The dependences of noise spectral density on the magnetic field are shown in Fig. 3 for T = 300 K and T = 200 K. The symbols are the experimental dependence of noise at the frequency of the analysis f = 10 Hz. The data are shown for two temperatures. The continuous solid and dashed lines represent the results of the calculations using eqn (8). The value of the residual noise level is taken as the same for both temperatures: $C = 1.9 \times 10^{-10}\ Hz^{-1}$. The solid lines correspond to R_c = 0 Ω while the dashed lines are obtained for the R_c values extracted from the I–V characteristics. The contact resistance represents the upper bound and it is most likely overestimated. Therefore, the actual dependence of noise on the magnetic field falls into the interval between the solid and dashed lines.

The first important observation from Fig. 3 is that eqn (8) well represents the decrease in noise in weak magnetic fields. In excellent agreement with the assumption of the mobility fluctuations as an origin of the $1/f$ noise, the magnetic-field dependence of noise has a pronounced minimum at approximately $\eta\xi\mu_{app}$ = 1. This is the first observation of noise decrease under conditions of geometrical magnetoresistance which proves the mobility fluctuations as a source of the noise. The minor discrepancy can be attributed to the

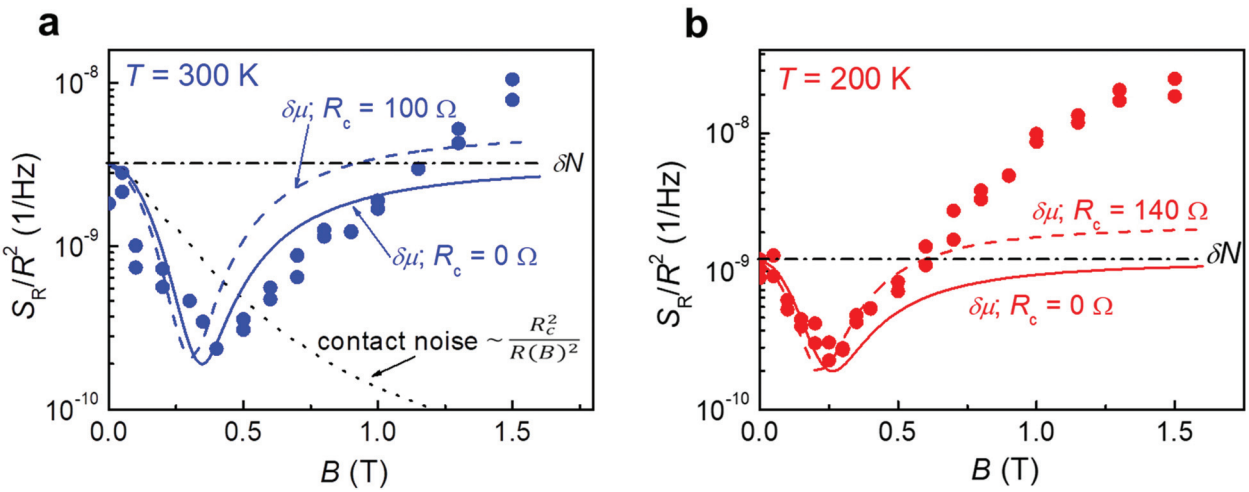

Fig. 3 Relative noise spectral density as a function of the magnetic field. The results are shown for graphene at (a) T = 300 K and (b) T = 200 K under the condition of the geometrical magnetoresistance in FETs with the channel's aspect ratio W/L = 4. The symbols show the experimental results for the frequency of analysis f = 10 Hz. The solid and dashed lines are the calculations assuming the mobility fluctuations as a dominant source of the $1/f$ noise. The solid line corresponds to the R_c = 0 Ω. The dashed line corresponds to the upper bound of the contact resistance extracted from the current–voltage characteristics. The dotted and dash-dotted lines show the hypothetical noise behavior in the cases of the contact noise and noise due to the fluctuations in the number of carriers, respectively.

unknown contact resistance and deviation from the quadratic magnetoresistance. Note, that we should not expect a perfect match of the experiment and calculations for the position of the noise minimum because, as one can see from Fig. 2b, the magnetoresistance deviates from the quadratic dependence at high magnetic fields. Although eqn (8) reproduces well the overall magnetic field dependence of noise, the higher the magnetic field the less the agreement between the experimental data and the model. This is predictable because in high magnetic fields the magnetoresistance strongly deviates from the $[R(B) - R(0)]/R(0) \sim B^2$ law.

There are several reasons for the strong increase of noise in high magnetic fields. First, in the high magnetic field, electrons are pushed to one of the side edges of the channel. Edge states might give a higher contribution to noise. Second, the current crowding at the rectangular sample corners gives an enhanced contribution to noise.

To add the final element to the conclusion about the noise nature, we have to exclude a possible contact origin of the noise. If noise originates from the contact resistance fluctuations, the noise spectral density of the total resistance fluctuations can be obtained from the analysis of the channel and contact resistors series connection

$$\frac{S_R(B)}{R(B)^2} = \frac{S_{Rc}}{R_c^2}\frac{R_c^2}{R(B)^2} \quad (9)$$

where $S_{Rc}/{R_c}^2$ is the relative spectral noise density of the contact resistance fluctuations, which does not depend on the magnetic field. In Fig. 3a, the dotted line shows the dependence calculated using eqn (9) and experimental dependence $R(B)$. As seen, the assumption of the contact resistance noise does not agree with the experiment either in weak or strong magnetic fields.

Conclusions

For the first time since the discovery of the $1/f$ noise hundred years ago, we have proven conclusively that the fluctuations in the mobility of charge carriers can be the dominant mechanism of the $1/f$ noise. We utilized the unique geometry and high electron mobility of graphene to directly assess the mechanism of the low-frequency electronic current fluctuations. In order to do this, the noise was measured as a function of the magnetic field strength under the condition of geometrical magnetoresistance. It was found that the relative noise spectral density of the graphene resistance fluctuations depends non-monotonically on the magnetic field with a minimum at $\mu_0 B \cong 1$. This observation proves unambiguously that mobility fluctuations are the dominant mechanism of the low frequency noise in graphene. Our results are important for all proposed applications of graphene in electronics, since the $1/f$ noise is the dominant contributor to phase noise in electronic communication systems and limits the sensitivity and selectivity of electronic sensors. The significance of our finding goes beyond the graphene field by adding to the fundamental understanding of $1/f$ noise: mobility fluctuations like carrier number fluctuations can indeed have the relevant time constants for dominating the noise spectrum at low frequencies.

Experimental methods

Heterostructure fabrication and characterization

Graphene field-effect transistors were fabricated from graphene-based heterostructures. Fabrication of the graphene heterostructures started from the mechanical exfoliation of monolayer graphene and two relatively thick hexagonal boron nitride (*h*-BN) flakes on a SiO_2/Si substrate with 300 nm SiO_2. To achieve larger size graphene flakes, the Si/SiO_2 substrate was exposed to an oxygen plasma (50 W, 120 s), and thereupon the surface of the tape was brought into contact with the SiO_2 surface. As the next step, the substrate was annealed on the hot plate for 2 min at 100 °C and after cooling down the sample to room temperature the tape was removed. Finally, the substrate was examined under the optical microscope to identify the graphene flakes (Fig. S2a†). Oxygen plasma pretreatment of the substrates was not necessary for the exfoliation of the *h*-BN flakes as we were able to find large enough *h*-BN flakes (Fig. S2b and c†). Both *h*-BN flakes were characterized by a Stylus Profilometer. We found a thickness of ~20 nm for the top *h*-BN and ~30 nm for the bottom *h*-BN.

The graphene-based heterostructure was fabricated by using a polymer dry-transfer technique, similar to the method for assembling van der Waals heterostructures reported elsewhere.[41] The stamp to pick-up and transfer the required 2D flakes was prepared by using a homemade polycarbonate (PC) solution (6.5% dissolved in chloroform) and a polydimethylsiloxane (PDMS) block. The staking process starts as follows: the top *h*-BN flake was picked up and then transferred onto the graphene sheet to initially fabricate an *h*-BN/graphene heterostructure. After that, the *h*-BN/graphene heterostructure was cleaned in chloroform for a few minutes to remove the PC residues. The process was repeated and the heterostructure was picked up and transferred onto the bottom *h*-BN to fabricate the final *h*-BN/graphene/*h*-BN van der Waals heterostructures (see Fig. S3a†). The resulting van der Waals heterostructures were characterized by Raman spectroscopy (micro-Raman spectrometer LabRAM HR Evolution) using a 532 nm laser with an incident power of approximately 1 mW. The typical Raman spectrum is shown in Fig. S3b.†

Device fabrication

The device fabrication process followed the procedure described in detail in ref. 42 and 43 The fabricated heterostructure was first patterned using electron beam lithography (EBL) and a homemade PMMA (5% in chlorobenzene) as a resist to define two bars with widths (W) of 16 μm and 20 μm (Fig. S4a†). The heterostructure was dry-etched for 20 seconds in an ICP-RIE Plasma Pro Cobra 100 under an SF_6 atmosphere (40 sccm, P = 75 W and T = 10 °C) and the areas uncovered by

a PMMA, used as a mask, were removed. Then, the graphene based heterostructure bars were cleaned in acetone and isopropanol for a few minutes to remove the remaining PMMA and checked using an optical microscope (Fig. S4b†). The drain and source contacts were patterned by a second round of e-beam lithography (Fig. S5a†), and thereupon, the sample was dry-etched once again to open access to the encapsulated graphene sheet. Our etching recipe provides a truncated square pyramid shape with a contact angle of approximately 40° to the horizontal plane ensuring high-quality quasi one-dimensional ohmic contacts with the encapsulated graphene. Finally, the sample was placed inside an e-beam evaporator where the metal drain and source contacts were made by evaporating at very low pressures (10^{-8} mbar)—3.5 nm of Cr (0.06 nm s^{-1}) and 55 nm of Au (0.25 nm s^{-1}). The final device, after a lift-off process in acetone, is shown in Fig. S5b.† The drain and source contacts were patterned with a meander shape in order to increase the contact length and minimize the contact resistance.

Current–voltage and noise measurements

The current–voltage characteristics and noise spectra were measured inside a closed cycle cryogenic probe station (Lake Shore Inc. CRX-VF). The noise was measured with the source and gate grounded. The signal from the drain load resistor (R_L) was amplified and analyzed by a spectrum analyzer. To minimize the power supplier noise, we used a battery biasing circuit to apply voltage bias to the devices. The noise spectral density of the drain voltage fluctuations (S_V) was converted to the current (S_I/I^2) and resistance (S_R/R^2) relative noise spectral densities as:

$$\frac{S_I}{I^2} = \frac{S_R}{R^2} = S_V\left(\frac{R_L + R}{R_L R}\right)^2 \frac{1}{I^2}$$

Data availability

The data that support the plots within this paper and the other findings of this study are available from the corresponding author upon reasonable request.

Author contributions

M. L. and S. R. conceived the idea of noise measurements in graphene in a magnetic field. A. R. and S. R. planned and performed the measurements. J. A. D. N., J. S. S., and M. M. fabricated and characterized the samples. G. C., W. K., and A. A. B. contributed to the noise data analysis. All authors participated in the manuscript preparation.

Conflicts of interest

The authors declare no competing interests.

Acknowledgements

The authors are very grateful to Prof. M. I. Dyakonov, who proposed the idea of noise measurements under magnetoresistance conditions in 1982. The work was supported by the CENTERA Laboratories in the framework of the International Research Agendas program for the Foundation for Polish Sciences, co-financed by the European Union under the European Regional Development Fund (No. MAB/2018/9). A. A. B. acknowledges the Vannevar Bush Faculty Fellowship award (class of 2021). M. M. acknowledges the support by the Spanish Ministry of Science, Innovation, and Universities and FEDER under the Research Grants numbers RTI2018-097180-B-100 and the FEDER/Junta de Castilla y León Research Grant numbers SA256P18 and SA121P20. J. A. D. N. also acknowledges the technical help from Dr Vito Clericò.

References

1 J. B. Johnson, *Phys. Rev.*, 1925, **26**, 71.
2 A. Van der Ziel, in *Advances in electronics and electron physics*, Elsevier, 1979, vol. 49, pp. 225–297.
3 R. F. Voss, in *33rd Annual Symposium on Frequency Control*, 1979.
4 P. Dutta and P. Horn, *Rev. Mod. Phys.*, 1981, **53**, 497.
5 M. Weissman, *Rev. Mod. Phys.*, 1988, **60**, 537.
6 R. F. Voss and J. Clarke, *Phys. Rev. Lett.*, 1976, **36**, 42.
7 A. L. McWhorter, in *Semiconductor Surface Physics*, ed. R. H. Kingston, University of Pennsylvania Press, Philadelphia, 1957, p. 207.
8 V. Shadrin, V. Mitin, V. Kochelap and K. Choi, *J. Appl. Phys.*, 1995, **77**, 1771–1775.
9 Z. Gingl, C. Pennetta, L. Kiss and L. Reggiani, *Semicond. Sci. Technol.*, 1996, **11**, 1770.
10 J. Xu, D. Abbott and Y. Dai, *Microelectron. Reliab.*, 2000, **40**, 171–178.
11 A. Geremew, C. Qian, A. Abelson, S. Rumyantsev, F. Kargar, M. Law and A. A. Balandin, *Nanoscale*, 2019, **11**, 20171–20178.
12 A. Szewczyk, Ł. Gaweł, K. Darowicki and J. Smulko, *Energies*, 2021, **14**, 8340.
13 M. Levinshtein and S. Rumyantsev, *Sov. Phys. Semiconduct.-USSR*, 1983, **17**, 1167–1169.
14 H.-J. Lippmann and F. Kuhrt, *Z. Naturforsch., A: Astrophys., Phys. Phys. Chem.*, 1958, **13**, 474–483.
15 T. Jervis and E. Johnson, *Solid-State Electron.*, 1970, **13**, 181–189.
16 P. Blood and R. J. Tree, *J. Phys. D: Appl. Phys.*, 1971, **4**, L29.
17 M. H. Song and H. Min, *J. Appl. Phys.*, 1985, **58**, 4221–4224.
18 M. H. Song, A. Birbas, A. van der Ziel and A. van Rheenen, *J. Appl. Phys.*, 1988, **64**, 727–728.
19 Y.-S. Kim, S.-S. Yun, C. H. Park, H. S. Min and Y. J. Park, *Solid-State Electron.*, 2004, **48**, 641–654.
20 S. Rumyantsev, M. Shur, N. Dyakonova, W. Knap, Y. Meziani, F. Pascal, A. Hoffman, X. Hu, Q. Fareed and Y. Bilenko, *J. Appl. Phys.*, 2004, **96**, 3845–3847.

21 N. Dyakonova, S. Rumyantsev, M. Shur, Y. Meziani, F. Pascal, A. Hoffmann, Q. Fareed, X. Hu, Y. Bilenko and R. Gaska, *Phys. Status Solidi A*, 2005, **202**, 677–679.
22 M. Kirton and M. Uren, *Adv. Phys.*, 1989, **38**, 367–468.
23 K. S. Novoselov, A. K. Geim, S. V. Morozov, D.-E. Jiang, Y. Zhang, S. V. Dubonos, I. V. Grigorieva and A. A. Firsov, *Science*, 2004, **306**, 666–669.
24 Y. Zhang, Y.-W. Tan, H. L. Stormer and P. Kim, *Nature*, 2005, **438**, 201–204.
25 A. K. Geim and K. S. Novoselov, in *Nanoscience and technology: a collection of reviews from nature journals*, World Scientific, 2010, pp. 11–19.
26 A. A. Balandin, *Nat. Nanotechnol.*, 2013, **8**, 549–555.
27 S. Rumyantsev, G. Liu, W. Stillman, M. Shur and A. Balandin, *J. Phys.: Condens. Matter*, 2010, **22**, 395302.
28 Y. M. Galperin, V. Karpov and V. Kozub, *Adv. Phys.*, 1989, **38**, 669–737.
29 A. Dmitriev, M. Levinshtein and S. Rumyantsev, *J. Appl. Phys.*, 2009, **106**, 024514.
30 S. Rumyantsev, G. Liu, W. Stillman, M. Shur and A. A. Balandin, *J. Phys.: Condens. Matter*, 2010, **22**, 395302.
31 M. Zahid Hossain, S. Rumyantsev, M. S. Shur and A. A. Balandin, *Appl. Phys. Lett.*, 2013, **102**, 153512.
32 F. Giubileo, A. D. Bartolomeo, N. Martucciello, F. Romeo, L. Iemmo, P. Romano and M. Passacantando, *Nanomaterials*, 2016, **6**, 206.
33 A. Cultrera, L. Callegaro, M. Marzano, M. Ortolano and G. Amato, *Appl. Phys. Lett.*, 2018, **112**, 093504.
34 T. Wu, A. Alharbi, T. Taniguchi, K. Watanabe and D. Shahrjerdi, *Appl. Phys. Lett.*, 2018, **113**, 193502.
35 S. Rumyantsev, D. Coquillat, R. Ribeiro, M. Goiran, W. Knap, M. Shur, A. Balandin and M. Levinshtein, *Appl. Phys. Lett.*, 2013, **103**, 173114.
36 Y.-W. Tan, Y. Zhang, H. L. Stormer and P. Kim, *Eur. Phys. J.: Spec. Top.*, 2007, **148**, 15–18.
37 D. K. Efetov and P. Kim, *Phys. Rev. Lett.*, 2010, **105**, 256805.
38 F. Giubileo and A. D. Bartolomeo, *Prog. Surf. Sci.*, 2017, **92**, 143–175.
39 P. Alekseev, A. Dmitriev, I. Gornyi and V. Y. Kachorovskii, *Phys. Rev. B: Condens. Matter Mater. Phys.*, 2013, **87**, 165432.
40 M. Kamada, V. Gall, J. Sarkar, M. Kumar, A. Laitinen, I. Gornyi and P. Hakonen, *Phys. Rev. B: Condens. Matter Mater. Phys.*, 2021, **104**, 115432.
41 P. Zomer, M. Guimarães, J. Brant, N. Tombros and B. Van Wees, *Appl. Phys. Lett.*, 2014, **105**, 013101.
42 J. Delgado-Notario, V. Clericò, E. Diez, J. Velázquez-Pérez, T. Taniguchi, K. Watanabe, T. Otsuji and Y. Meziani, *APL Photonics*, 2020, **5**, 066102.
43 V. Clericò, J. A. Delgado-Notario, M. Saiz-Bretín, A. V. Malyshev, Y. M. Meziani, P. Hidalgo, B. Méndez, M. Amado, F. Domínguez-Adame and E. Diez, *Sci. Rep.*, 2019, **9**, 1–7.